12-2-2016

Structural Reinforcement through Liquid Encapsulation

Alin Cristian Chipara

Peter Samora Owuor

Sanjit Bhowmick

Gustavo Brunetto

S. A. Syed Asif

See next page for additional authors

Authors

Alin Cristian Chipara, Peter Samora Owuor, Sanjit Bhowmick, Gustavo Brunetto, S. A. Syed Asif, Mircea Chipara, Robert Vajtai, Jun Lou, Douglas S. Galvao, and Chandra Sekhar Tiwary

DOI: 10.1002/((please add manuscript number))

Article type: Communication

Structural Reinforcement Through Liquid Encapsulation

Alin Cristian Chipara†, Peter Samora Owuor†, Sanjit Bhowmick, Gustavo Brunetto, Syed Asif, Mircea Chipara, Robert Vajtai, Douglas S. Galvao, Chandra Sekhar Tiwary*, Pulickel M. Ajayan**

Alin Cristian Chipara, Peter Owuor, Robert Vajtai, Chandra Sekhar Tiwary, Pulickel M. Ajayan

Department of Materials Science and Nanoengineering, Rice University, Houston, Texas 77005, United States

E-mail: cst.iisc@gmail.com, ajayan@rice.edu

Sanjit Bhowmick, Syed Asif,

Hysitron, Inc., Minneapolis, Minnesota 55344, United States

Gustavo Brunetto, Douglas S. Galvao

Instituto de Física "Gleb Wataghin", Universidade Estadual de Campinas, CP 6165, 13083-970 Campinas, Sã o Paulo, Brazil

E-mail: galvao@ifi.unicamp.br

Mircea Chipara,

Department of Physics and Geology, The University of Texas Rio Grande Valley, Edinburg,

Texas 78539, United States

Keywords: solid-liquid interface; *in-situ* mechanical testing; PDMS-PVDF; DFT calculation; MD simulation.

Introduction:

In contrast to conventional composite materials design, liquid structural reinforcement in solid materials has not attracted a lot of attention from researchers, although nature is abundant with liquid reinforced materials. The natural occurring solid-liquid system inspired design of liquid filled composite as a self-healing composites,[1–5] conductive networks[6,7] and thermal networks[8]. Recently, Style *et. al.*[9] designed and explained the concept of liquid reinforced composites following the work of Eshelby[10] using glycerol liquid inclusions in a silicone matrix. They showed a high dependence of surface tension with stiffness. The addition of a liquid into a solid matrix can have a drastic change in the mechanical response of materials[9].

In conventional composites, the improvement of mechanical properties depends on stress transfer (or strain accommodation) from the matrix to the reinforcement[11]. Hence, in the past a large effort has been made to engineer the interface that

can utilize the properties of reinforcements. Surface modification, morphological engineering of the reinforcement, and the addition of surface binders are a few of the common methods of improving load bearing capability and interfacial strength of such composites[11–17]. In the case of solid-liquid composite materials, the viscosity of the reinforced liquid is important since the flow of the liquid under load determines the shape of the solid shell, which can result in a unique load transfer mechanism which is very different from conventional composites[9,18–20]. Apart from the size and surface tension of the reinforcement, the interface between the liquid and solid plays a crucial role in determining unique mechanical properties such as stress absorption, or strain accommodation in the composite[21]. In this work, we show that two well-known polymers can be used to design a new type of composite where significant structural reinforcement can be achieved through liquid encapsulation. This new approach represents a shift in the concepts about structural reinforcement and expands on the work of Style *et al.*[9] by using a much stiffer matrix and a modified liquid filler which gives rise to novel pathways and materials that would previously be disregarded. Recently, work from our group showed how a mobile and liquid interfaces can help a material adapt to stresses[22]. This mechanism can be exploited more broadly to create stronger and more resilient materials.

In the current work, we explore load bearing ability of liquid/solid interface by synthesizing liquid filled microspheres. The microspheres consist of two ideal immiscible polymer systems; polydimethylsiloxane (PDMS) filled polyvinylidenefluoride (PVDF) capsules. Hydroxyl terminated PDMS was chosen as the filler due to the huge flexibility of its polymer backbone, whereas PVDF was chosen due to its strong chemical resistivity and high mechanical modulus value[23,24]. The *in-situ* compression inside a Scanning Electron Microscope (SEM) was used to investigate the deformation

mechanisms of the microspheres. In order to gain further insight into these mechanisms, we have also carried out density functional theory (DFT) and fully atomistic molecular dynamics (MD) simulations.

Results and Discussion

In **Figure 1**a we present the scalable and simple process for the synthesis of PDMS/PVDF spheres with average sizes between 30 and 40 microns. The detailed procedure is discussed in the experimental section of the manuscript. Scanning electron microscope (SEM), transmission electron microscope (TEM), and focused ion beam (FIB) were used to obtain the structural data of the microspheres. An SEM image of a cluster of the spheres, as shown in Fig. 1b, exhibits homogeneous shape and size. **Figure 1**c shows a FIB image of a single sphere. Once a section of the sphere is FIB milled (**Figure 1**d), the liquid spreads out of the shell (**Figure 1**e). Additionally, the thickness of the solid shell varies with the size of the spheres, in most cases thickness is $1/20^{th}$ of the radii. Representative TEM imaging show that spheres of PDMS/PVDF (having ~300 nm radius) have a PVDF shell that is only ~15 nm thick (**Figure 1**f). The FIB of larger spheres shows the shell thickness and liquid inside the solid sphere. A detailed size analysis of the spheres shows the size varies from 300 nm up to 30 µm. SEM analysis shows 80-90 percent of particles range from 10-30 microns in size. The simulated structure of the sphere is shown in **Figure 1**g (more details in the methods section), which is obtained by stabilizing molecular structure of PDMS and PVDF into a sphere. The simulations showed that mixing these two polymers lead to the formation of a structurally rigid PVDF outer shell encapsulating a liquid phase (PDMS), which is in good agreement with the

experimental data. The elemental analysis by Dong *et al.*[22] on similar materials revealed that fluorine atoms are preferentially located on the shell of the microspheres while silicon atoms are found within the microspheres. This further supports the expected core-shell structure with a fluid core of PDMS and a solid external shell of PVDF.

The mechanical response of the spheres was characterized through a variety of tests including dynamic mechanical analysis (DMA) and *in-situ* compression testing. Macroscale DMA mechanical tests of sphere aggregated at room temperature cold press showed that the high stiffness is retained through several cycles (**Figure 2**a). The load-unload data showed some secondary peaks, which can be attributed to slip and structural re-arrangement of the spheres. During each loading cycle, the spheres are re-organized into a more tightly packed configuration as reflected in the changes in stiffness values. They return to an equilibrium state during or after unloading. This suggests that the spheres do not permanently deform, but instead distribute the load evenly. As expected, the stiffness values increase as the static force increases. The macro-scale data shows stiffness values of 12 kN/m. This behavior reveals the effectiveness of solid-liquid composites for dissipating energy or load which can total or at least partially recover their initial configuration after unloading. The high stiffness exhibited by the PDMS/PVDF spheres may be explained by the content of liquid within the spheres. In order to understand the deformation of the individual solid sphere filled with liquid, the *in-situ* testing was performed using a 30 µm flat punch with an SEM PicoIndenter (Hysitron Inc.). The results are shown in **Figure 2**b-d. Load versus depth plots of uniaxial compression of a single sphere are shown in **Figure 2**b. One plot shows deformation of the sphere (up to 7000 µN) and then unloading (deformation 1) and the other shows deformation until shell fracture (deformation 2). The

elastic modulus is calculated using the loading curve and is found to be 354 kPa. The SEM images acquired during deformation are shown in **Figure 2**c.

The deformaion mechanism of the solid-liquid sphere can be understood by considering two springs with different stiffnesses in series. (**Figure 2**e). Lets consider that the spring constant of the shell is K_S and the spring contant of the liquid is K_L. Both elements experience a similar load (*P*), since the load is uniaxial. However, the strain will be distributed by the equations, $\varepsilon_{total} = \varepsilon_s + \varepsilon_L$. As the stifness of the liquid ($K_L = P/\varepsilon_L$) is much lower than that of the solid ($K_S = = P/\varepsilon_S$), the strain in the liquid will be much higher resulting in a change in the shape of the particle to accommodate the large strain. In response to applied load, the sphere deforms into an elliptical shape (side view) thereby taking the majority of the load away from the solid shell. In solid-solid composites, interfacial failure is common due to modulus mismatch, whereas in the case of solid-liquid composites, the liquid flows as dictated by the solid shape and can accommodate large strains without interfacial cracking. After unloading (release of load), the particle returns to its original spherical shape after 10 seconds since there was no permanent deformation of the shell. In-order to keep the minimum energy shape (spherical), the liquid flows back once the pressure is released (**Figure 2**e).

In the second loading (deformation 2), the sphere was compressed until fracture. The sphere yields at a load of 8000 µN, corresponding to a stress of ~12 MPa. The sphere fracture takes place at a load of 11500 µN, i.e. 16.3 MPa and a strain of 80%. The energy calculated using the area under the force-displacement curve is 0.2 J. A time lapse of the behavior of the response of the spheres to load and their subsequent failure can be seen in **Figure 2**d. After yielding, the sphere deforms plastically and a crack initiates at the surface in the orthogonal direction of the loading as shown by the arrow

and schematic inset. The liquid component of the material can be seen coming out in the final image in **Figure 2**d.

In order to gain further insight on the atomic-level mechanisms behind the sphere structural reinforcements, we carried out fully atomistic molecular dynamics (MD) simulations (details are provided in simulation details section)[25–30]. We investigated the structural and dynamic properties of composites made up of a mixture of PVDF and PDMS polymeric chains. Two cases were considered; (i) a composite composed of a mixture of PDMS and PVDF in equal amounts (in weight) and initially randomly distributed; and (ii) a two-phase system composed of a hollow sphere made of PVDF and filled by PDMS. During the compression cycle of the mixture we analyzed the Coulomb interactions between PVDF and PDMS. More specifically, we analyzed the interactions between the fluorine atoms, from PVDF, with the hydrogen atoms, from PDMS (see structures displayed in **Figure 3**a). At the compression stage of the first cycle, the polymer chains are densified (are placed in closer contact) and the energy contribution associated with the Coulomb interactions decreases to ~6000 kcal/mol (**Figure 3**b). When the piston returns in the next cycle, due to its periodic motion, this energy changes, from -6000 to around -4000 kcal/mol and stabilizes through the next cycle. During the second compression cycle, the Coulombic energy drops from -4000 to -7000 kcal/mol, indicating that the F – H interactions increase, as a result of the structural rearrangement of the composite induced by the piston movements, followed by a new structural stability plateau with energy around -5000 kcal/mol. After the third compression cycle, the minimum energy stabilizes around -7000 kcal/mol when the piston is compressing the system and around -5200 kcal/mol when the pressure is released. The corresponding von Mises stress and hydrostatic pressure values are presented in **Figure 3**c-d, respectively. From the MD simulations we observed the formation of spheres with the

external shell composed mostly of PVDF, with encapsulated PDMS (**Figure 1**g and **Figure 3**e-f), which is consistent with the experimental observations (**Figure 1**). In order to test these sphere structural stabilities and whether the used model can describe a two-phase system, we carried out an MD within an NVT ensemble with the constant temperature of 300 K. With no external forces acting on the system, the spheres remained stable for up to 2 ns. Due to the liquid behavior of the PDMS, it can deform to fulfill the hollow space in the center of the sphere (see video 01 – Supplementary information). Additionally, it is noticeable that the PDMS can occupy some holes present in the PVDF shell structure. The hydrostatic pressure in the material was also modeled and showed that the PVDF-PDMS mix withstood up to 500 atm of pressure in each cycle (**Figure 3**d). The Coulomb energy evolution showed that the interaction between PDMS and PVDS during the compression process becomes stronger (**Figure 3**d). Thus, one mechanism that may improve the PVDF cluster formation is the Coulomb interaction between the two phases of the composite. We also modeled the von Mises stresses in the material whilst undergoing compression and it showed irreversible stresses deformations being built into the material with each cycle and a maximum stress of 11000 atm (**Figure 3**c). The material did not exhibit instant recovery but a viscoelastic relaxation to a new equilibrium point (~8000 atm). The general features (shape and pattern) of the stress curves from these simulations are very similar to those from the experimental studies. Additionally, the hydrostatic pressure patterns presented in **Figure 3**d reinforces our failure hypothesis discussed in the *in-situ* measurements. In order to gather further insight in the interpretation of the *in-situ* results, we have also carried out a molecular dynamics simulations of the compression (squeeze) of a single sphere and calculated its corresponding stress-strain curve. Our results show that as the sphere moves from a stable configuration (**Figure 3**e) and starts to become compressed (**Figure 3**f)

most of the strain is transferred to its liquid center (see also video 01). At a strain of 30%, we observe the formation of a crack at the surface orthogonal to loading direction very similar to that of the experimental observation. Although the size and loading rates are different in the experiments and the simulation due to computational limits, we are still able to capture the deformation of the solid liquid system. The section of the sphere during loading shows most of the strain is taken by the liquid and expands in all three directions. After yielding, the surface solid cracks, the liquid does not move out of the solid shell due to interfacial interactions and the surface tension forces. In conventional reinforced (with a good interface) composites, with hard reinforcements (high modulus), load transfers from the matrix to the reinforcement and fails as the interface or matrix. Due to mismatch in the strain of the matrix and reinforcement, cracks initiate at either the interface or in the matrix and fractures subsequently. In liquid reinforced composites, the spheres deform and load transfers from the solid to the soft liquid (negligible modulus) and results in an increase in stiffness due to the incompressibility of the liquid phase. As the loading increases the interface changes and due to viscosity the liquid changes its shape and fits the surface. Due to such a high interface matching of solid and liquid, the spheres deform almost 80% before yielding. The atomic interaction at the interface and high viscosity of the liquid does not allow the liquid phase to pass through the cracks and is able to continue loading.

In order to fully utilize the unique mechanical behavior of the spheres, we embedded the spheres in PDMS (a two-part Sylgard 184). The full procedure is described in the experimental section of this manuscript. The inset in **Figure 4**a shows PDMS composite samples with spheres (first 3 vials) and the pure PDMS control (rightmost clear vial). When comparing the behavior of the neat spheres to those inside of the PDMS matrix the general profile looks similar. However, in this case,

the spheres are well protected by the PDMS matrix. Thus, they are able to take much larger loads and this leads to a larger overall stiffness. These mechanical results are in agreement with previous stiffening seen by Bartlett *et al.* for liquid metal inclusions[7]. In **Figure 4**a-b a set of SEM images of the reinforced PDMS matrix after straining can be seen. It is quite clear from this figure that the spheres act as points of deflection. The crack lines can be clearly followed in both **Figure 4**a-b and are highlighted in the inset in **Figure 4**b. In this figure, we see the crack lines stopping at the spheres and having to changed directions. This takes a great deal of energy and increases the durability of this material by a large amount. Due to the energy required for cracks to do this, the spheres can stop cracks from propagating through the rest of the material and thus allowing the material to hold its properties through higher stresses. The liquid nature of the inside of the spheres adds to this behavior by allowing them to absorb a lot of energy. This is emphasized by the maximums seen in **Figure 4**c-f. The stiffness of the sphere-reinforced PDMS increases by 32.4% and 72.3% for 20% and 50% loading, respectively (see **Figure 4**d). This is quite a large increase considering the spheres reinforcing the matrix are mostly liquid. We also modeled the behavior of the material in response to a force ramp (**Figure 4**e). Both pure PDMS and the reinforced matrix show similar trends. However, as the sphere content increases so does the maximum stiffness values. Although this material doesn't show behavioral changes in the force ramp, there is remarkable change when we apply a constant load the material (**Figure 4**d). The material was cycled constantly at 5 Hz and a difference in the stiffness behavior is clear. As more spheres are added the material begins to exhibit increased stiffening, or self-stiffening as described by others[9,22,31,32]. Self-stiffening has generally been seen when performing isothermal tests with a multitude of cycles over time. The behavior can appear due to incomplete curing or even due to structural re-arrangement. In the reinforced

composite, this behavior is most likely due to the interaction between the compression and the liquid pushing back against the force. The liquid PDMS prefers to assume a spherical shape since that is the configuration of lowest energy. However, whilst being deformed it pushes back causing a rise in stiffness. Additionally, the more spheres are present the more the shells have an effect on the overall stiffness. Moreover, if the PVDF shells of the spheres touch they will also cause an apparent increase in the overall stiffness. This behavior is clearly not seen in the pure PDMS control and is only apparent as the wt. % of spheres increases. As such, this effect is not due to curing since all materials were cured under the same conditions. After analyzing the data of the various tests a very clear linear trend can be seen in relation to wt. % of spheres (**Figure 4**f). To highlight this trend we employed a bar graph. The bar graph clearly shows a positive linear trend which is also supported by the fact that the 20 wt. % sample since almost exactly halfway between the pure PDMS and the 50 wt. % sample. This means that we should be able to tune the stiffness to whatever values we want between the two points. To better understand the mechanical behavior as a function of temperature we set up a temperature ramp test in the DMA. PDMS showed a steady increase in stiffness with temperatures up to 200^0C. However, after the spheres are added the behavior shows a drastic change and a dip at about 150^0C (**Figure 4**c). This is due to the melting of the PVDF and the loss of structure, which causes the stiffness to drop dramatically. This is confirmed by the difference in the drops observed between the 20 wt. % sample and the 50 wt. % sample.

Conclusion

In summary, the synthesis a new PVDF-PDMS composite that contains liquid PDMS and surrounded by shell of solid PVDF has been reported. The material exhibits an interesting mechanical behavior and shows promise as a reinforcing agent even while containing nearly 60 % liquid. The *in-situ* mechanical testing shows unique deformation behavior. Molecular models reinforce the mechanical analysis and show the same dynamics as seen in the experimental results. Also, the simulation shows interface between solid-liquid plays an important role in strain accommodation, load bearing capacity and fracture behavior. Moreover, the simulations show that some of the novel properties of the reinforced PDMS are strongly dependent on the level of Coulomb interactions, which can be exploited to tune the stiffness of this new class of materials. The novel sphere with solid-liquid can be used as reinforcement and shows self-stiffening and improvement in mechanical properties. The synthesis of these materials can also be used as a starting point for advanced applications such as drug delivery, impact resistance, acoustics, or in creating hierarchical materials[33–35].

Experimental details

Synthesis of spherical composite:

To synthesize the polymer encapsulated liquid shells, we followed a similar procedure to the one reported by Dong *et al.* [22]. We took PVDF (Alfa Aesar, 23,500−29,500 poise) and dissolved into THF (tetrahydrofuran) while under magnetic stirring. The solution was monitored until it reached homogenization (approximately 3 hours). After the PVDF solution reached homogenization hydroxyl terminated PDMS (Sigma-Aldrich, 18,000- 22,000 cSt) was added. The mixture was allowed to stir for approximately 1 hour. Afterwards the mixture was put into a fume hood and tip sonicated and magnetically stirred simultaneously until all solvent was removed (approximately 24 hours). The final

ratio of PDMS to PVDF was 62:38 wt. %, based on initial material added (20.4786 g PVDF with 33.577 g PDMS). The material was removed and left to fully dry in air for a day. In order to fully remove the solvent, the as-obtained composite was heat-treated above the boiling point of THF (100°C) for 24 hours.

Incorporation PVDF/PDMS spheres into PDMS matrix:

We used Sylgard 184 (Dow Corning) and added 20 wt. % and 50 wt. % spheres into Part A of the PDMS and then added the crosslinking agent in a 1:10 ratio. The samples were cured in vacuum at 60°C. The curing in vacuum was done to eliminate air bubbles. The hydroxyl terminated PDMS did not cure using the same curing agent and thus the innermost part of the spheres remained liquid thus making this system truly unique.

Dynamic Mechanical Analysis:

All DMA measurements were done using a DMA Q800 from TA Instruments. To measure the pure spheres, the powder containing them was taken and placed in a rectangular shape. The area was measured and used for the runs. The load-unload runs varied in maximums between the spheres (0.15 N, 0.5 N, 1 N) and the composites (1 N, 2 N, 5 N, 10 N, 15 N). The composites were run at a constant rate of 0.5 N/min whilst the spheres were run at 0.15 N/min for the first two load unload cycles then 0.1 N/min for the final cycle. The isothermal measurements were done at a constant frequency of 5 Hz and a temperature of 30°C with a 20 micron oscillation amplitude. The force ramp used in the testing went up to 18N at a rate of 0.5 N/min. The thermal ramp used in the testing went up to 200°C at a rate of 3°C/min.

Microscopy:

FIB was done using an FEI Helios SEM/FIB. SEM was done using FEI Quanta 400 ESEM at scanning electricity of 15 to 20 kV. Transmission electron microscope (TEM) was done on JEOL 2100 Field Emission Gun. *In-situ* compression tests were carried out using an SEM PicoIndenter, PI 85 (Hysitron, Inc.)

Simulation Details:

The polymers were described using Compass force field[25] for the bonded terms and Buckingham potential[26,27] to describe long-range interaction. All the used parameters are described in the references[28–30]. A typical structure obtained from MD simulations is presented in **Figure 1**d (external view and cross section). These structures were obtained considering an initial configuration of spherical shells of PVDF (outer layer) and PDMS (inner one). The system is then geometrically optimized and led to the structures shown in **Figure 1**g. No demixing was observed for the cases we considered. We investigated different starting configurations and the final results were not very sensitive to the initial configurations. The obtained configurations are structurally robust and consistent with the experimental data.

In order to study dynamic response under mechanical deformation, the structures were subject to compression by an external piston executing a harmonic movement. Up to 3 complete oscillations with a period of 200 ps were considered. Due to computational limitation, a small sphere of 10 nm is used for compression, keeping the fraction of solid and liquid similar to that used in the experiments.

Supporting Information

Supporting Information is available from the Wiley Online Library or from the author.

Acknowledgements

Authors acknowledge the funding support from U.S. Department of Defense: U.S. Air Force Office of Scientific Research for the Project MURI: "Synthesis and Characterization of 3-D Carbon Nanotube Solid Networks" Award No. etFA9550-12-1-0035. GB and DSG acknowledge Computational and financial support from the Center for Computational Engineering and Sciences at Unicamp through the FAPESP/CEPID Grant No. 2013/08293-7. The authors also gratefully acknowledge funding support from the Air Force Office of Scientific Research (FA9550-13-1-0084).

Received: ((will be filled in by the editorial staff))
Revised: ((will be filled in by the editorial staff))
Published online: ((will be filled in by the editorial staff))

References

[1] M. D. Hager, P. Greil, C. Leyens, S. Van Der Zwaag, U. S. Schubert, *Adv . Mater* **2010**, *22*, 5424.

[2] D. S. Xiao, Y. C. Yuan, M. Z. Rong, M. Q. Zhang, *Polymer (Guildf).* **2009**, *50*, 2967.

[3] J. Yang, M. W. Keller, J. S. Moore, S. R. White, N. R. Sottos, *Macromolecules* **2008**, *41*, 9650.

[4] T. Yin, M. Z. Rong, M. Q. Zhang, G. C. Yang, *Compos. Sci. Technol.* **2007**, *67*, 201.

[5] S. R. White, N. R. Sottos, P. H. Geubelle, J. S. Moore, M. R. Kessler, S. R. Sriram, E. N. Brown, S. Viswanathan, *Nature* **2001**, *409*, 794.

[6] A. Fassler, C. Majidi, *Adv. Mater.* **2015**, *27*, 1928.

[7] M. D. Bartlett, A. Fassler, N. Kazem, E. J. Markvicka, P. Mandal, C. Majidi, *Adv. Mater.* **2016**, *28*, 3726.

[8] S. H. Jeong, S. Chen, J. Huo, E. K. Gamstedt, J. Liu, S.L. Zhang, Z.B. Zhang, K. Hjort, Z. Wu, *Sci. Rep.* **2015**, *5*, 18257.

[9] R. W. Style, R. Boltyanskiy, B. Allen, K. E. Jensen, H. P. Foote, J. S. Wettlaufer, E. R. Dufresne, *Nat. Phys.* **2014**, *11*, 82.

[10] J. D. Eshelby, *Proc. R. Soc. A Math. Phys. Eng. Sci.* **1957**, *241*, 376.

[11] P. M. Ajayan, L. S. Schadler, C. Giannaris, A. Rubio, *Adv. Mater.* **2000**, *12*, 750.

[12] N. C. Beck Tan, S.K. Tai, R. M. Briber, *Polymer (Guildf).* **1996**, *37*, 3509.

[13] A. Eitan, K. Jiang, D. Dukes, R. Andrews, L. S. Schadler, *Chem. Mater.* **2003**, *15*, 3198.

[14] J. D. Achenbach, H. Zhu, *J. Mech. Phys. Solids* **1989**, *37*, 381.

[15] A. C. Balazs, T. Emrick, T. P. Russell, *Science* **2006**, *314*, 1107.

[16] K. Hu, D. D. Kulkarni, I. Choi, V. V Tsukruk, *Prog. Polym. Sci.* **2014**, *39*, 1934.

[17] T. Mirfakhrai, J. D. W. Madden, R. H. Baughman, *Mater. Today* **2007**, *10*, 30.

[18] R. Höhler, S. Cohen-Addad, *J. Phys. Condens. Matter* **2005**, *17*, 1041.

[19] A. Fery, R. Weinkamer, *Polymer (Guildf).* **2007**, *48*, 7221.

[20] L. Wang, J. Lau, E. L. Thomas, M. C. Boyce, *Adv. Mater.* **2011**, *23*, 1524.

[21] C. Zhong *et al., Nature Nanotech*. **2014**, *9*, 858.

[22] P. Dong, A. C. Chipara, P. Loya, Y. Yang, L. Ge, S. Lei, B. Li, G. Brunetto, L. D. Machado, L. Hong, Q. Wang, B. Yang, H. Guo, E. Ringe, D. S. Galvao, R. Vajtai, M. Chipara, M. Tang, J. Lou, P. M. Ajayan, *ACS Appl. Mater. Interfaces* **2016**, *8*, 2142.

[23] A. P. Sokolov, V. N. Novikov, Y. Ding, *J. Phys. Condens. Matter* **2007**, *19*, 205116.

[24] A. Vinogradov, F. Holloway, *Ferroelectrics* **1999**, *226*, 169.

[25] H. Sun, *J. Phys. Chem. B* **1998**, *5647*, 7338.

[26] R. A. Buckingham, *Proc. R. Soc. A Math. Phys. Eng. Sci.* **1938**, *168*, 264.

[27] F. Jensen, *Introduction to Computational Chemistry*, John Wiley & Sons, West Sussex, England **2007**, pp. 22-77.

[28] D. R. Dillon, K. K. Tenneti, C. Y. Li, F. K. Ko, I. Sics, B. S. Hsiao, *Polymer (Guildf).* **2006**, *47*, 1678.

[29] N. Karasawa, W. A. Goddard, *Macromolecules* **1992**, *25*, 7268.

[30] J. S. Smith, O. Borodin, G. D. Smith, *J. Phys. Chem. B* **2004**, *108*, 20340.

[31] A. Agrawal, A. C. Chipara, Y. Shamoo, P. K. Patra, B. J. Carey, P. M. Ajayan, W. G. Chapman, R. Verduzco, *Nat. Commun.* **2013**, *4*, 1739.

[32] B. J. Carey, P. K. Patra, L. Ci, G. G. Silva, P. M. Ajayan, *ACS Nano* **2011**, *5*, 2715.

[33] T. Brunet, A. Merlin, B. Mascaro, K. Zimny, J. Leng, O. Poncelet, C. Aristégui, O. Mondain-Monval, *Nat Mater* **2015**, *14*, 384.

[34] R. S. Lakes, *J. Compos. Mater.* **2002**, *36*, 287.

[35] C. C. Muller-Goymann, *Eur. J. Pharm. Biopharm.* **2004**, *58*, 343.

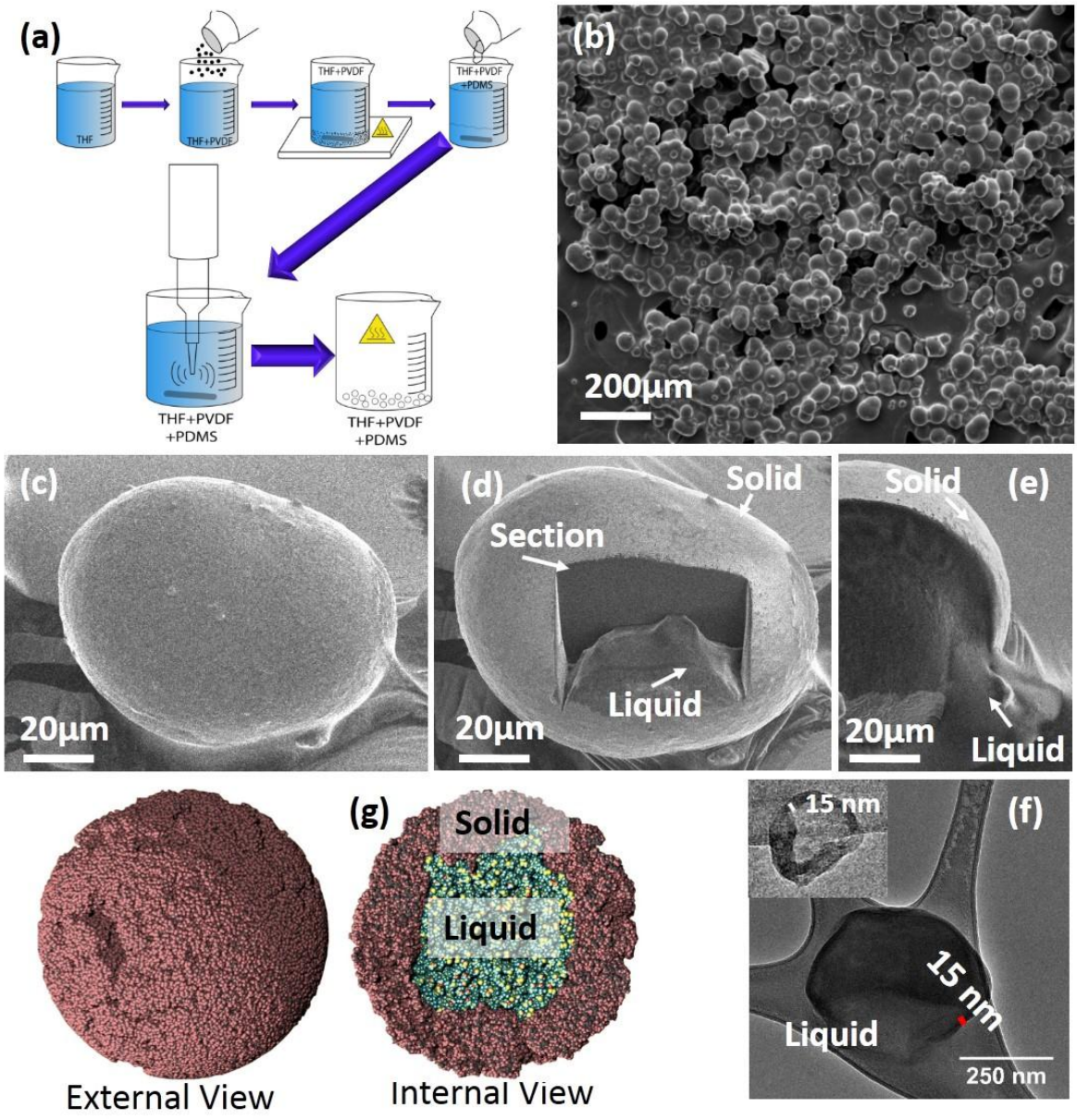

Figure 1: Morphology of the liquid spheres a) Scheme of the process to create the PVDF encapsulated PDMS. b) SEM image of a cluster of the spheres; c) shows an FIB image of one sphere d) then the sphere after an incision e) and finally the liquid flowing and spreading out of the incision. f) TEM image of a 0.5µm burst sphere where the wall is calculated to be 15 nm and there is a clear

contrast between the outer solid shell and liquid polymeric phase inside the sphere. g) Obtained simulated structural model and its cross-section. Mixing PDMS/PVDF results in a structure where the PVDF composes a rigid outer layer encapsulated a liquid PDMS phase.

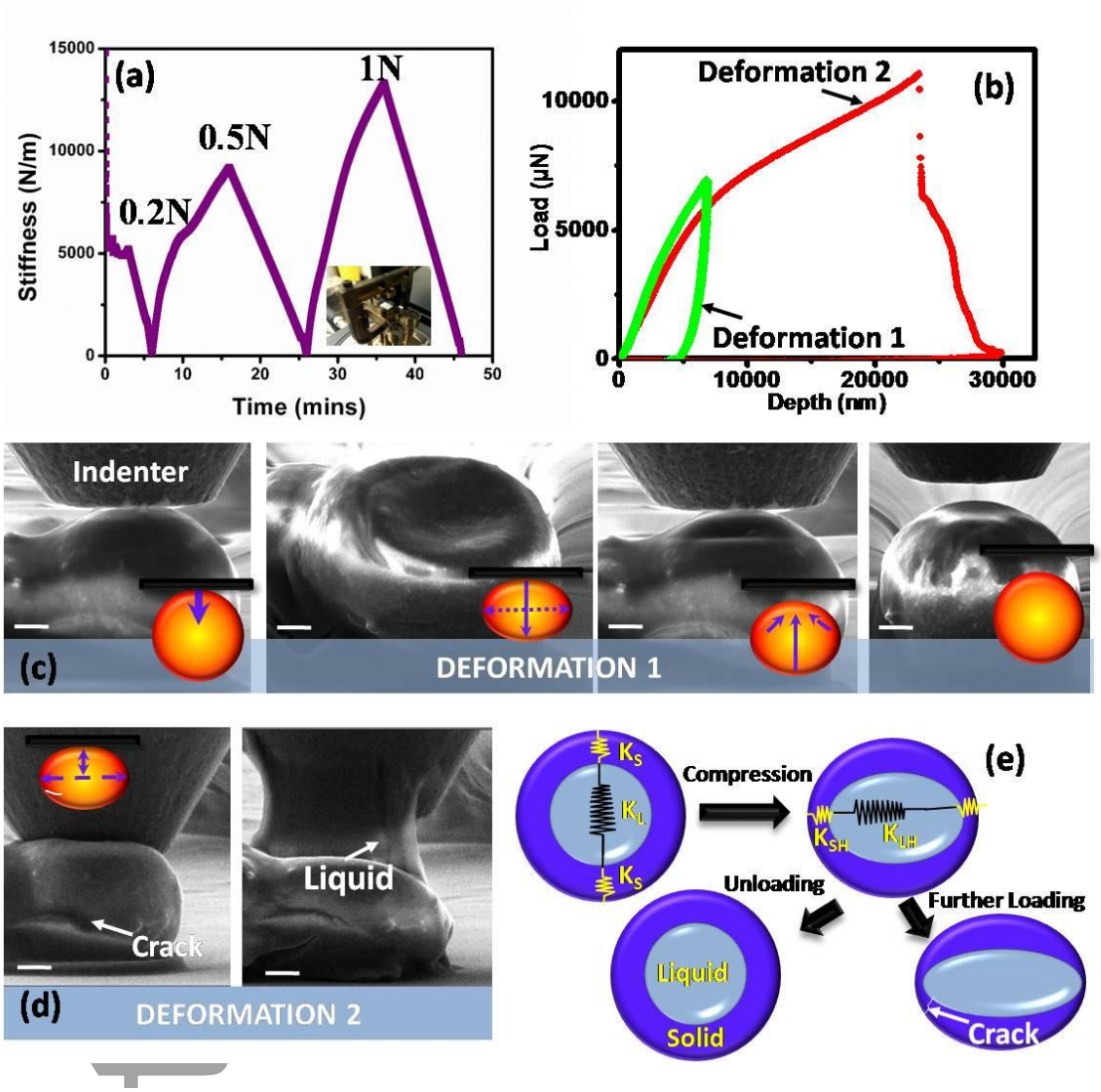

Figure 2: Mechanical behavior of a single PDMS/PVDF sphere a) Sphere stiffness values as a function of time at regimes of 0.2 N, 0.5 N, and 1 N, as obtained from load-unload testing using a DMA Q800.

The inset in shows the spheres after their mechanical testing. b) Shows the load versus depth curve of the *in-situ* SEM testing of a single sphere. The images below c) correspond to the *in-situ* testing of the spheres. Shows the spheres prior to load and the spheres after loading. d) Shows a time lapse of the behavior of the spheres once pressure is applied and once they eventually burst and then the pressure is removed. e) Unique behavior of solid-liquid sphere observed in current work.

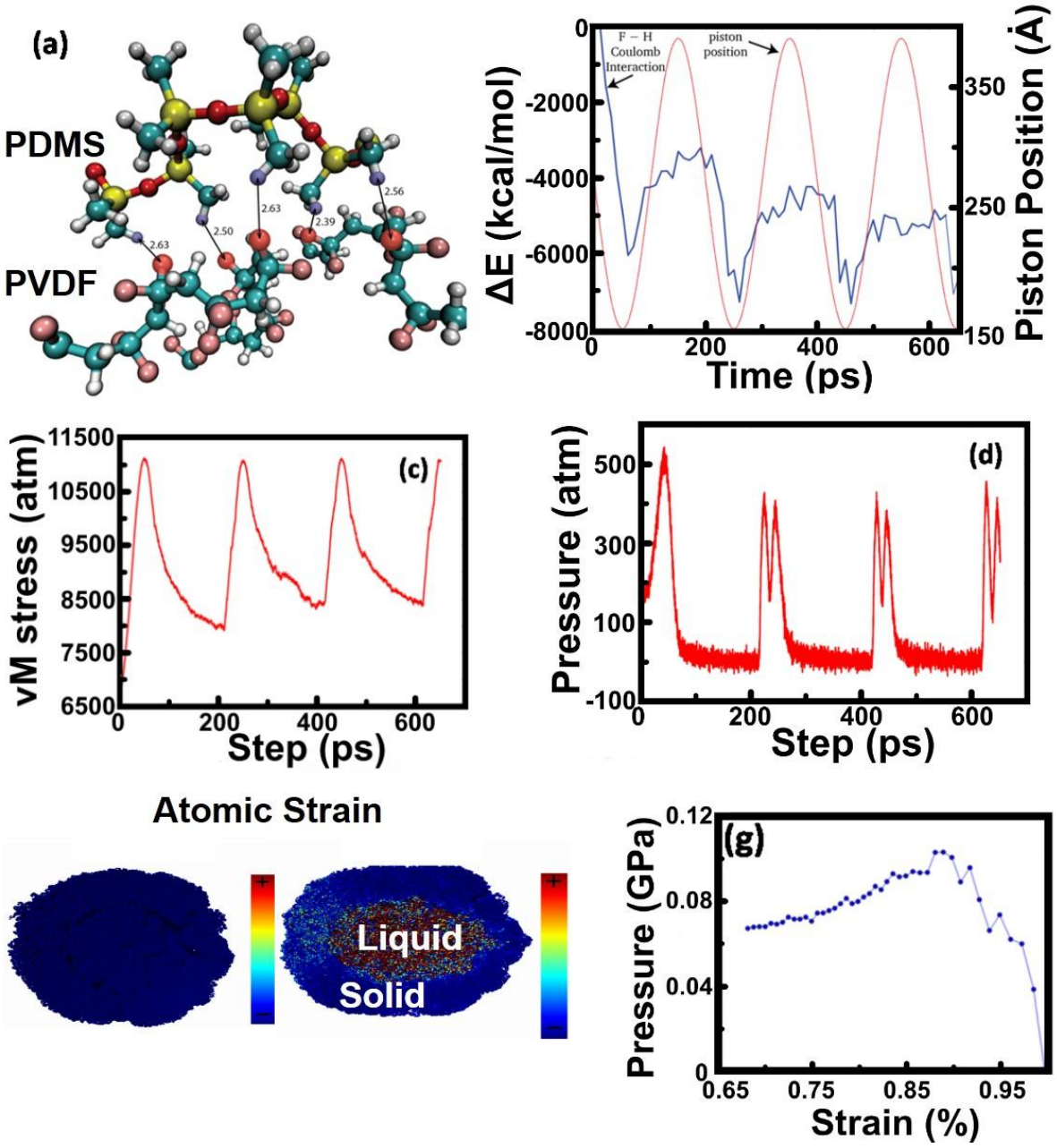

Figure 3: Theoretical modeling of PVDF/PDMS spheres a) Optimized structural model of PVDF and PDMS chains. The most important atoms (F and H) and distances for the Coulombic interactions are also clearly marked; b) variation of the Coulombic energy (blue curve) as a function of the simulation time. The corresponding piston positions in indicated in the red curve; c) von Mises stress values in

the spheres as a function of simulation time and d) hydrostatic pressure values experienced by the sphere as a function of the simulation time; e) Structural two-phase sphere model and the correspond atomic strain values for the uncompressed (left) and compressed (right) stages, respectively; f) Pressure values experienced by the two-phase sphere model as a function of the applied compression (strain). A corresponding quantitative stress-strain plot can be seen in g).

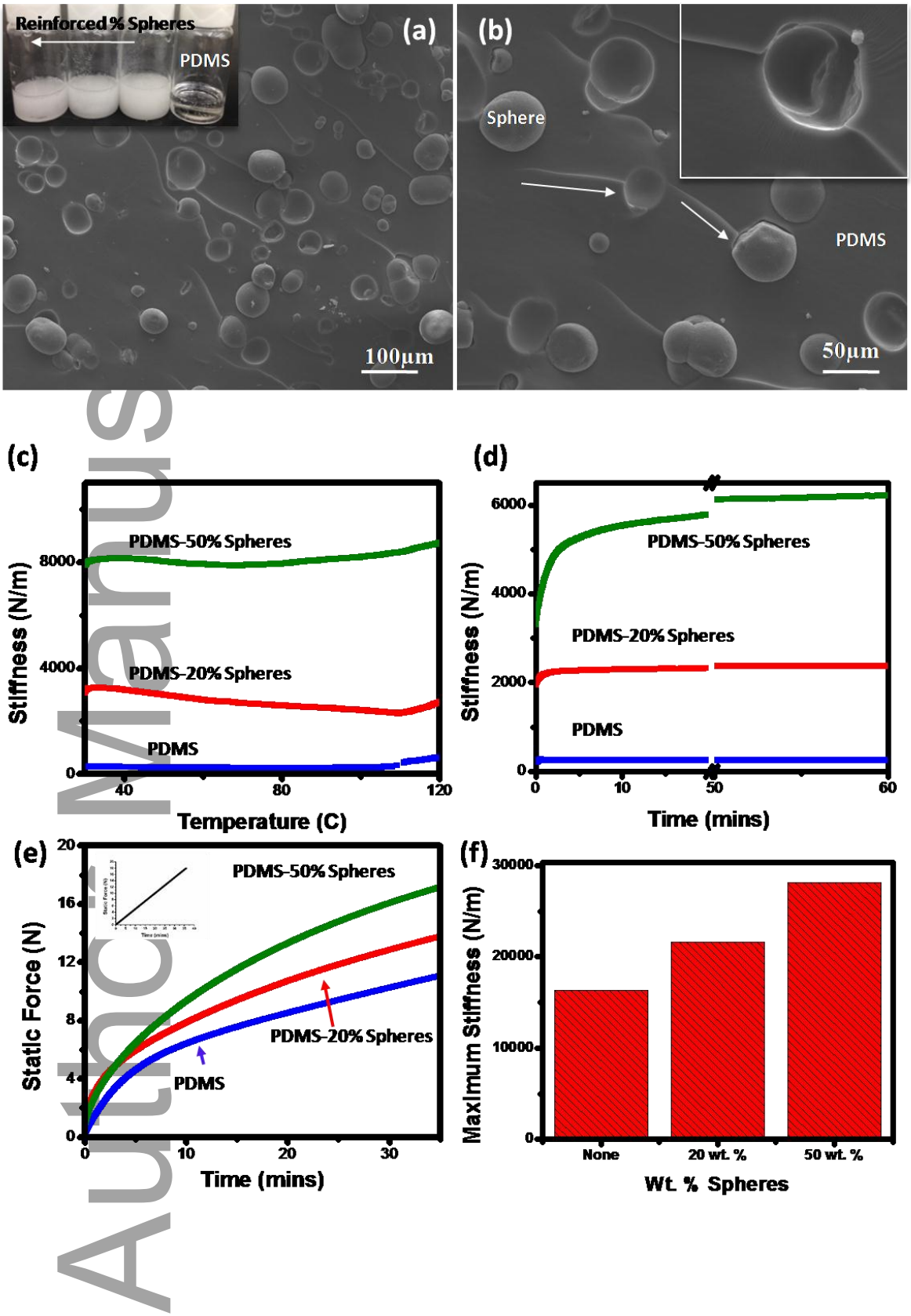

Figure 4: Testing and imaging of sphere-reinforced PDMS composites a) Images of different solutions of PDMS as an inset (rightmost clear bottle) and SEM images of PDMS with the sphere reinforcement. b) Shows a detailed SEM image of the stress lines around the PDMS sphere and deflection of cracks that happens with the spheres present in the composite. c) Shows the behavior of pure PDMS (blue) and PDMS with 20 wt. % PVDF encapsulated PDMS (red) and 50 wt. % PVDF encapsulated PDMS (green) as a function of temperature. d) Shows the stiffness as a function of time in an isothermal test (same coloring scheme and wt. % as Fig. 4c) with dynamic compressive cycling. Finally, e) shows the response of the composites and pure PDMS to a compressive force ramp (inset in figure) and f) showing the effect that liquid has on the stiffness of the PDMS matrix with increasing wt. % of polymer encapsulated liquid.

The liquid inside a solid material is one of the most common composite materials in nature. The interface between solid-liquid plays an important role in unique deformation. Here, model systems of two polymers (PDMS-PVDF) are used to make sphere of solid with liquid inside it. We have used both experiential (*in-situ* mechanical testing) and theoretical calculation (DFT and MD) to understand such interfaces.

Keywords: solid-liquid interface, *in-situ* mechanical testing, PDMS-PVDF, DFT calculation, MD simulation

Structural Reinforcement Through Liquid Encapsulation

Alin Cristian Chipara [†], Peter Samora Owuor [†], Sanjit Bhowmick, Gustavo Brunetto, Syed Asif, Mircea Chipara, Robert Vajtai, Douglas S. Galvao, Chandra Sekhar Tiwary*, Pulickel M. Ajayan**